Modal Engineering for MEMS Devices: Application to Galvos and Scanners

Lawrence Barrett, Matthias Imboden, Joshua Javor, David K. Campbell and David J. Bishop, *Member, IEEE*

Abstract— **Optical systems typically use galvanometers (aka galvos) and scanners. Galvos move optical elements such as mirrors, quasi-statically, from one static position to another, and an important figure of merit is their step-settle relaxation time. Scanners move in an oscillatory fashion, typically at the device resonant frequency. MEMS devices, which have many advantages and are often used in such optical systems, are typically high Q devices. Moving from one position to another for a galvo or one frequency/amplitude to another for scanners, can take many periods to settle following the ring down. During these transitions, the optical system is inactive and the time is not being efficiently used. In this article we show how a novel class of open loop control algorithms can be used to rapidly change position, frequency and amplitude, typically in well under the period of the device. We show how the MEMS designer can excite, with complete, high-speed control, a vibrational mode of the system. We call this modal engineering, the ability to control the modes of the system in a practical, fast way. This control of the modes is accomplished with open loop control algorithms.**

Index Terms—**MEMS, Galvanometers, Galvos, Scanners, Modal Engineering, Step and Settle Time, Open Loop Controls**

I. INTRODUCTION

MEMS devices are playing a large and growing role in transducing the electronic domain into the mechanical [1-3]. In the world of MEMS actuators, devices that turn electrical controls into motion, modes of operation tend to fall into two broad classes. There is quasi-static operation where the device is moved from one static position to another and the figure of merit is the step and settle response time [4-9]. In optical systems, these types of devices are called galvanometers or "galvos".[1] The other typical mode of operation is scanning where the MEMS device continuously oscillates, usually at its resonant frequency, to leverage the Q of the system [10,11]. In optics, these types of devices are called "scanners" and can run along one or two axes. Here we discuss how they both can be operated with open loop control algorithms and achieve essentially ideal behavior.

These two types of operation, quasi-static and scanning, are widely used because they represent two stable states for a moderately high Q MEMS device, oscillating at resonance or being static [12,13]. The optical engineer can design the system to do something useful, such as imaging in a LIDAR system, while the device is doing one of these [14,15]. Using normal drive methods, transitioning from one of these states to the other requires waiting a multitude of periods of the device for the ringing behavior to end and this temporal overhead limits system performance. In this article, we show how a novel class of open loop control theory algorithms allow the MEMS designer to do modal engineering, e.g. the turning on and off of specific modes of the device with transitions between them that take only a fraction of a period. We believe these algorithms will open the design space and allow for practical MEMS devices that are hybrid in operation between galvos and scanners, as the benefits of a high Q system can be leveraged without the price of a slow response time, critical in many applications.

Figure 1 shows an example of what we discuss here. In the upper panel is shown the ability to turn the fundamental mode of the device on and off, precisely and quickly. This is a Simulink simulation for an infinite Q system with a 1 rad/sec resonant frequency. It would normally take an infinite time to make these transitions. As one can see, it is possible to abruptly turn these modes on and off, in integral units of the half period of the device. This is the behavior of an optimal scanner device. The lower panel shows how this same system can be made to operate quasi-statically, moving from one static position to another, quickly, with each transition taking one half of a period. Once again, this is for an infinite Q system. This is the behavior of an optimal galvo device. Combining these two methods lets one move the device to any position, to oscillate a specific number of cycles and then return to some other

L. Barrett is with the Division of Materials Science and Engineering, Boston University, Boston, MA 02215 USA. (e-mail: blawrenc@bu.edu).
M. Imboden is with the STI-IMT LMTS, École Polytechnique Fédérale de Lausanne, 2002 Neuchâtel, Switzerland (e-mail: m.imboden@gmail.com).
J. Javor is with the Department of Mechanical Engineering, Boston University, Boston, MA 02215 USA. (email: jjavor@bu.edu)
D. K. Campbell is with the Division of Materials Science and Engineering, Department of Electrical and Computer Engineering, Department of Physics, Boston University, Boston, MA 02215 USA. (email: dkcampbe@bu.edu)
D. J. Bishop is with the Division of Material Science and Engineering, Department of Electrical and Computer Engineering, Department of Physics, Department of Mechanical Engineering and Department of Biomedical Engineering, Boston University, Boston, MA 02215 USA. (email: djb1@bu.edu). Lawrence Barrett is the corresponding author.

[1] First galvanometers were used as current sensors, the name has been appropriated by systems where a mirror is moved by applying a current in order to position light. The sensor became an actuator.

position. We have demonstrated this performance in Figure 1 for an infinite Q system but our approaches are perfectly general and will work for any underdamped, second order system with a $Q>1$.
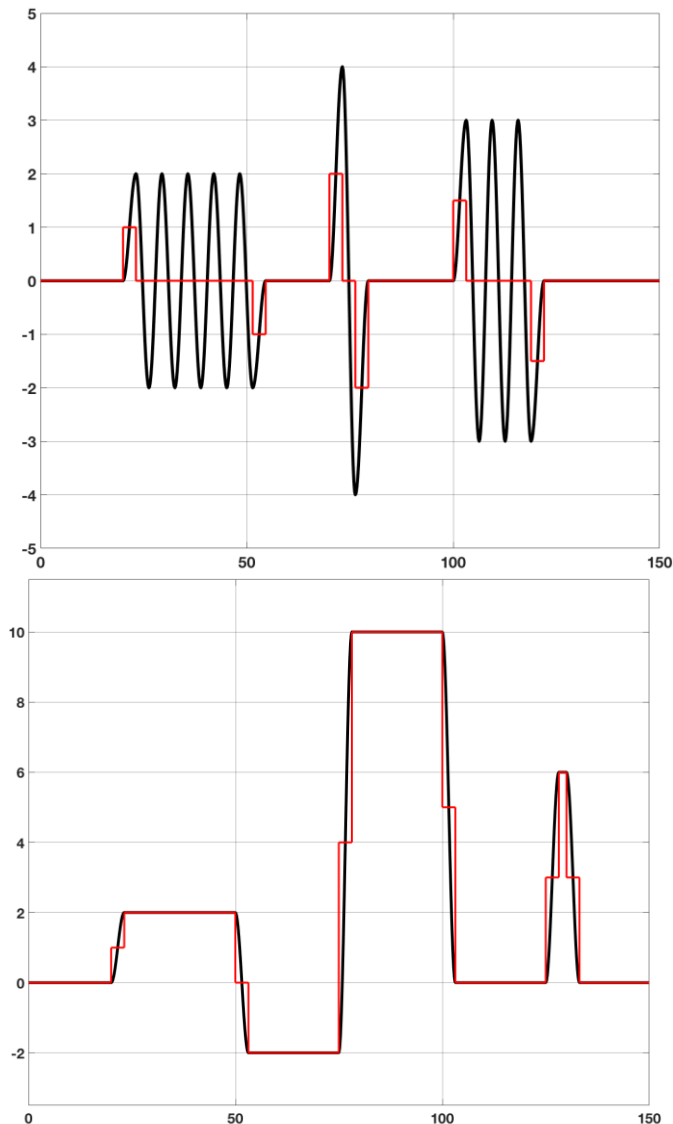

Figure 1 Shown in the upper panel is modal engineering, the ability to turn the modes of the system on and off, with precision. The lower panel shows ideal step and settle response for our system. Both results are for the same infinite Q system. The red curve is the applied drive and the black curve, the system response. This is a Simulink simulation.

II. BACKGROUND

In a previous set of papers [6,16-18] we have discussed the galvo behavior of a MEMS device and shown how it can have essentially perfect step and settle behavior. We will briefly summarize those results here. For a high Q system, when you apply a step function input, the system overshoots to twice the final rest position and then oscillates about that final rest position until it finally converges to that point. If, instead, a half-step is applied, one half a period later, the system is at a peak of its excursion with an amplitude equal to the desired final rest position. With zero slope in a position-time plot, its

velocity is zero. The method shown in Figure 1 applies half the value of the force needed to hold the device at its desired end position and after one half a period, applies the full force. With the device where it is intended to be, after half a period, with zero velocity, this application of the full force essentially catches it and holds it in the desired position, stably for as long is desired. This is called a double step (DS) drive. One half the force and one half the period are the values for an infinite Q ($Q>100$) system. This is perfectly general and works for a system with any Q with a modification of the parameters. This is derived later in the analytical section. Ref. 16 discusses a variety of similar drive schemes called overdrive methods where one applies an accelerating force for a while and then a decelerating force. They are similar to how one moves an object in free space where it starts at rest, an accelerating force is applied, and then a decelerating force is applied with the object arriving at its final rest position with zero velocity. The simulation shown in the lower panel of Figure 1 was obtained using DS for all the transitions. The drive signal is the red curve and one can see the double step structure for each transition. These open loop drive schemes allow for essentially ideal galvo behavior.

In this paper, our main focus is the behavior shown in the upper panel of Fig. 1. This is the effect we describe as modal engineering, the ability to turn the modes of the system on and off, quickly, with precision. The key to our approach is to drive the system coherently, with full knowledge of its underlying dynamics. In a conventional control theory approach [12,13], one uses feedback and methods like PID control. Our approach here is simpler from a system point of view because the sensor and feedback system are not needed, reducing cost and complexity. The high stability and linearity of MEMS make them ideally suited for such feedforward control algorithms [19].

This paper is organized into the following sections. In section IIA we present results from Simulink simulations using an infinite Q system, demonstrating all tools we have at our disposal. In section IIB we study a finite Q system showing how finite damping modifies the algorithms demonstrated in section IIA. In section III, we present a closed-form solution of the underlying equations of motion for our system. Finally, in section IV, we present experimental results on a MEMS micromirror. This analysis and data are for a MEMS application but we note that these approaches will work equally well for any underdamped, second order system.

A. Infinite Q Systems

In this section we discuss results obtained using Simulink simulations on an infinite Q, second order system. The system has a resonant frequency of 1 rad/sec, the period is 2π. The simulations are performed with time steps of 10^{-4} seconds and typically cover periods of time in the range of 100-300 seconds. If one gives the system a step input, one sees the behavior shown in Figure 2a). It rings forever, oscillating between zero and twice the nominal final resting place. A larger step increases the oscillating amplitude. If one turns the step off at an arbitrary time, the device ends up in a non-determinate state. The signal shown in Figure 2a) is unipolar, it oscillates between zero and twice the nominal resting point of the system. If one wishes to have bipolar behavior, one can use a pulse like that
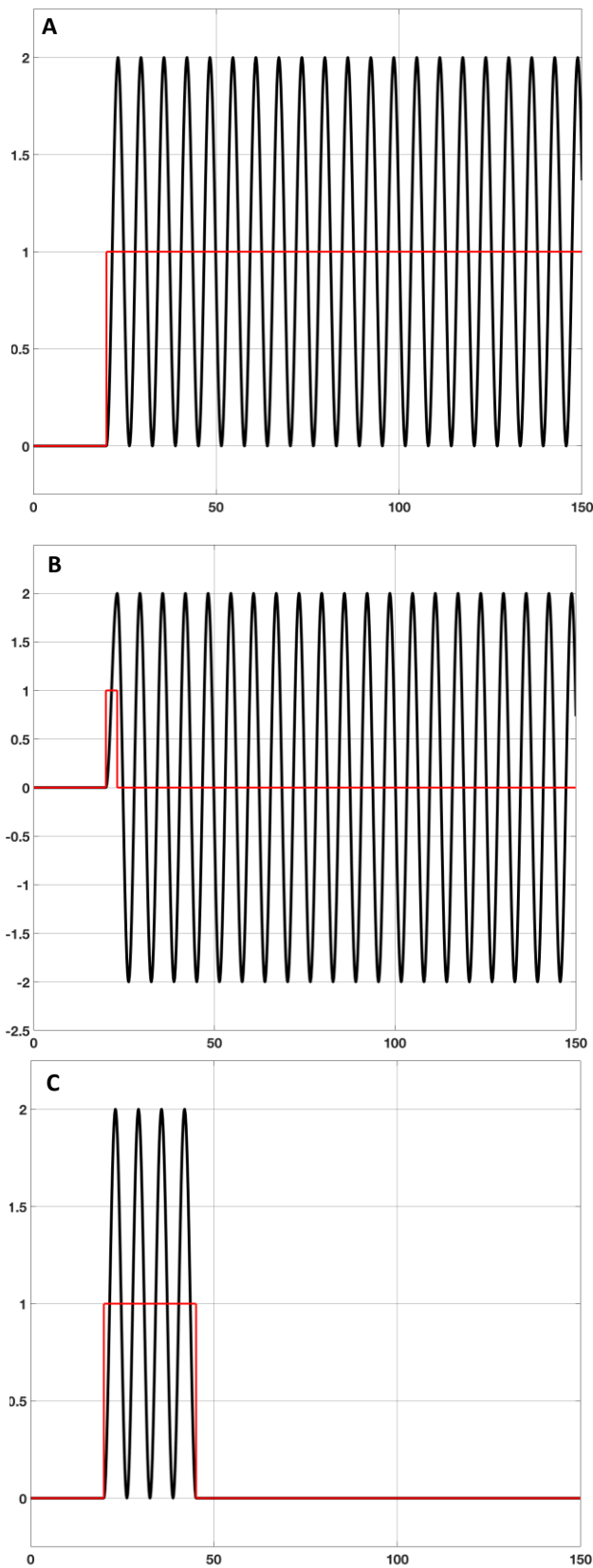
Figure 2 *Shown are Simulink simulations on an infinite Q system. On the upper panel is shown a response to a step. The system oscillates in a unipolar way, between zero and twice the equilibrium position. In the middle panel, when a half period pulse is applied, the system rings in a bipolar way. The lower panel shows turning the oscillations off by using a properly timed half period pulse.*

shown in Figure 2b). One half a period (π) after the step up, a step down in equal amplitude is applied. In this case the system oscillates symmetrically around zero.
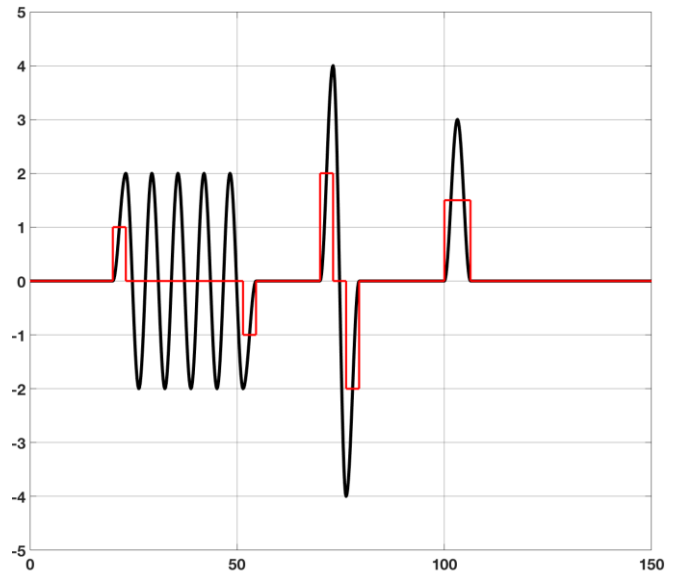

Figure 3 *Shown is how by combining the pulses, one can turn the modes on and off in myriad complex ways. The red traces are the applied drive and the black curves, the system response.*
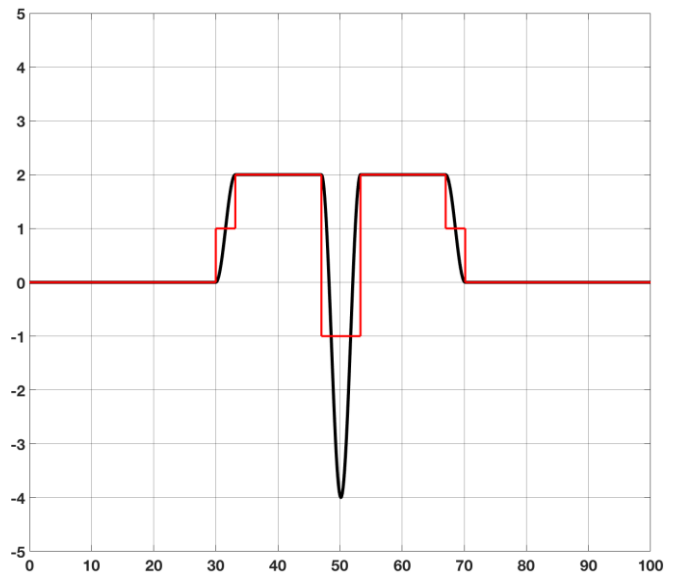

Figure 4 *Shown is an example of using double step (Fig. 1) and modal engineering (Fig. 3) to produce a complex response. This is a Simulink simulation for an infinite Q system. The red trace is the applied drive and the black curve is the system response.*

In 2c), we turn the step off 5 device periods (10π) after it starts. One can see that the modes have been completely and cleanly turned off. The key point is to apply the off pulse at a very specific time in the oscillation cycle to pull the energy out of the mode. We note that the system has an infinite Q but by using an understanding of the dynamics of the device, we can make it switch on and off in a single period. We also note these are open loop drive algorithms, there is no feedback being employed. The amplitude of oscillation is determined by the pulse amplitude.

As shown in Figure one can use a negative pulse applied an integer number of periods after the first pulse (in this case 5 periods or 10π) to turn the sequence off. One can have as few as one complete cycle or even a half a cycle. For the single full cycle, 1.5 periods long, one applies a step up, half a period later one has the step down to zero, half a period later a step down to minus the step-up amplitude and finally, a half a period later a step up to zero. To obtain the unipolar signal one applies a pulse of a full period length. When the system is at rest, a step up can be applied at any time. The key to the approach we present here is to apply the rest of the pulse sequence at times that correspond to integer values of the device period, which for MEMS devices may be known to 1 ppm or better. We are using an understanding of the device dynamics to time our pulses to let us turn these modes on and off at will. We refer to this capability as modal engineering.

For a linear system, one can combine the techniques shown in Figure 2 with those shown in Figure to produce complex patterns. An example of such a pattern is shown in Figure 4. In this figure, we use the DS drive (up and down) to create a plateau and then use the recipe for a full sine wave to put a put a negative pulse in the center of the plateau. With the tools presented here one can create an essentially unlimited set of patterns and behaviors of arbitrary complexity. One can engineer the modes of the MEMS device to meet the needs of the imaging system as opposed to designing the optics around the limitations of the MEMS device.

In this section, we have discussed the modal engineering of an infinite Q system. However, the techniques are general and can be applied to finite Q systems. In the next section we discuss these methods.

B. Finite Q Systems

For a system with a finite Q, one needs to modify the algorithms discussed previously in an appropriate way. Finite Q causes two effects, one trivial and one that must be dealt with. The trivial effect is the shift in resonant frequency due to finite damping. If one makes the standard correction, all is well. One needs to use the resonant frequency of the system for the timing as discussed above, which takes the dissipation into account. The second effect is somewhat more troubling and must be explicitly dealt with.

Finite Q means losses in the system from the oscillating mode. Figure 5 shows what happens. In the upper panel of Figure 5, the system has an infinite Q and behaves as described previously. In the lower panel, the system has a Q of ~100 and two things happen. Because energy is lost every cycle, the amplitude of the oscillating mode decays over time. And because the amplitude of the final cycle is not the amplitude of the first cycle, the negative going pulse pulls too much energy from the system and does not stop the response but causes it to oscillate at a non-zero amplitude. This loss of energy must be compensated for. To do this we add in a small amount of drive at the resonant frequency.

Figure 6 shows how this is done. We add in enough energy at the resonant frequency to compensate for the damping losses. We are, in essence, topping up the mode. This returns the response of the system to the ideal behavior seen for the infinite Q performance. The other drive techniques demonstrated for the infinite Q system can also be modified in a similar way.
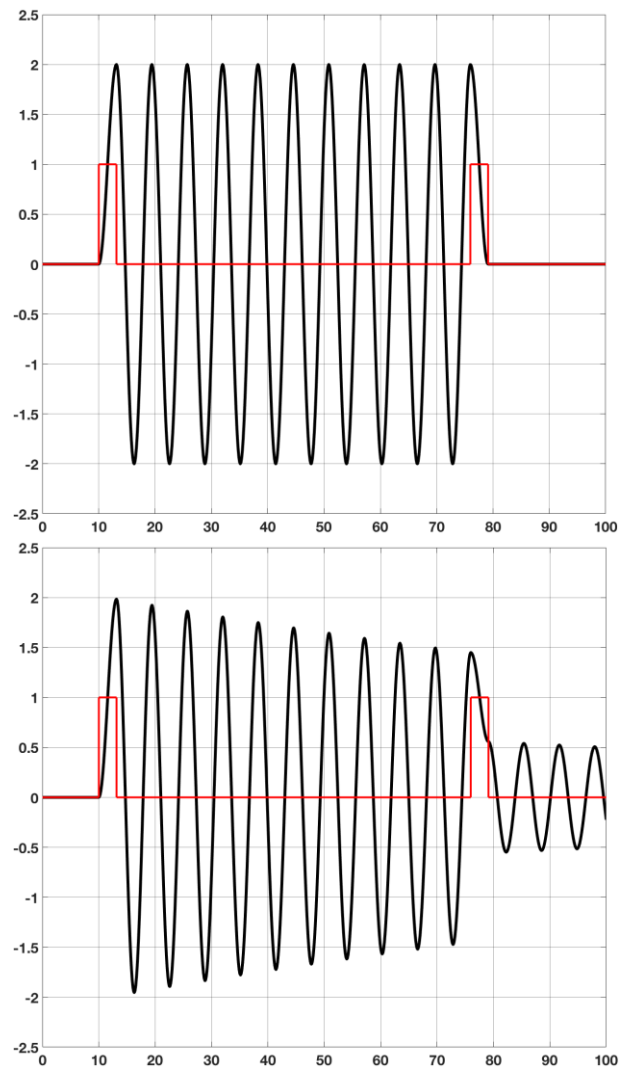

Figure 5 Shown is an 11 pulse cycle for an infinite Q system, upper panel and a system with a Q of 100, lower panel. These are Simulink simulations with the red traces the input and the black curves the system response.
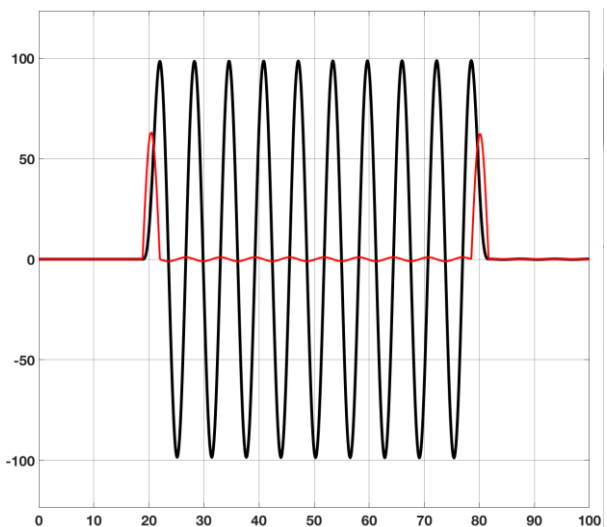

Figure 6 Shown is a Simulink simulation for a finite Q system (100) where we feed in enough AC signal to account for the damping losses after the initial pulse. Red: drive, black: response.
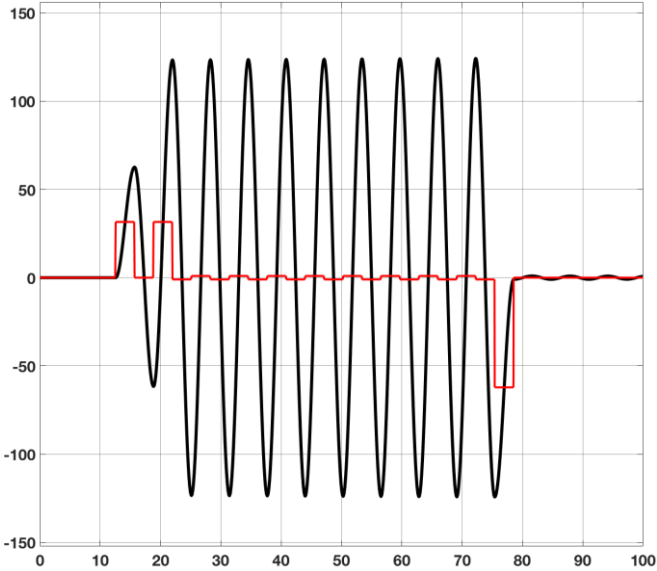
pulse which puts energy into the mode, a series of smaller pulses which keep the mode topped up to deal with the losses due to the finite Q of the system and finally an emptying pulse, which removes energy from the mode. The other type of drive

Figure 7 *Shown is a Simulink simulation of a system with a Q~100. Three new features are demonstrated: a) one can ring the system up (or down) in multiple pulses, b) we are using a square wave to keep the mode topped up and c) we can use a negative pulse, moved by ½ a period, to remove the energy from the mode. The red curve is the input and the black the response.*

In the infinite Q limit, the emptying pulse is equal in amplitude to the initial pulse. No energy is dissipated during the ringing of the system. For finite Q, the starting pulse is larger than the stopping pulse. This is because the starting pulse needs to add in some extra energy to account for the losses during the first cycle and the last pulse needs less energy because of losses during the last cycle. This equivalence is shown explicitly in the analytical section. Because one usually has a finite amount of force overhead to work with, a DC pulse is preferable because the power factor is 1 for a square pulse but only .707 for a sine pulse, requiring a larger force excursion for the same impulse.

Error! Reference source not found.7 shows a Simulink simulation with three new features. In the first, one can fill the mode initially (or empty it) using multiple timed pulses, with ~50% amplitude, one period apart. This may work better experimentally where the ability to apply large forces may be limited. In the second new feature, we use a unipolar square wave to keep the mode topped up. It works as well as the sine wave and simplifies the closed form analysis discussed in the next section. Finally, by shifting the emptying pulse by one half a period, one can use a negative going pulse instead of a positive pulse. These features allow one to tailor the drive to match the electronics and kinds of forcing one has available.

III. ANALYTICAL RESULTS

In this section, we discuss the analytical solution to the relevant ODE. As shown above, one can drive the system using either pulses or parts of sine waves. For the sake of simplicity, we discuss the use of pulses in this section. One thing we wish to do is to use the drives as shown in Figure 6. There is an initial
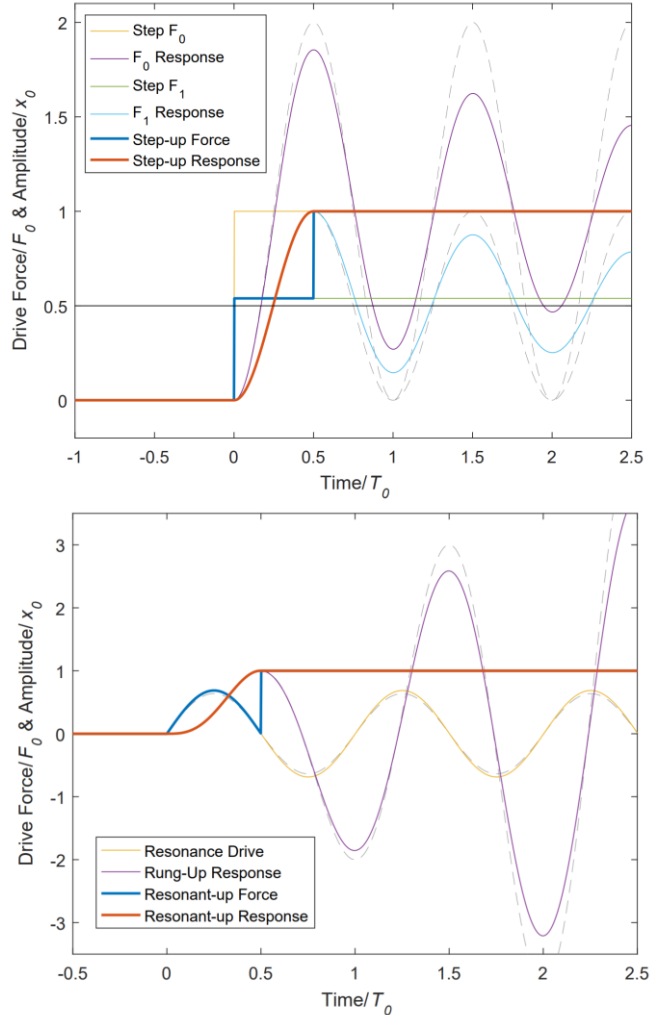

Figure 8 *Top: Shown is the single step and two-step response for a Q = 10 system (infinite Q response is dashed), calculated using the closed form solution 4 and 5. Bottom: resonant actuation for a Q=10 system (infinite Q response in dashed). In both plots the red trace depicts the set and hold response, illustrating a transition with no ringing or overshoot.*

we wish to use is the two-step drive, such as shown in Figure 8. All of these various drive schemes can be created by various combinations of step functions with appropriate time delays and changes in step height. Because our system is linear, we can create the complete analytical result of these complex drives by summing these various contributions to create our final system response. In this section, for simplicity, we focus on a system with finite $Q = \frac{m\,\omega_0}{\gamma}$ whose natural frequency is $\omega_0 = \sqrt{\frac{k}{m}}$, mass m and loss factor γ. The resonator is further characterized by its spring constant k and can be driven by static forces F_1 and harmonic forcing F_{dr} at a frequency of ω_{dr}. The resonance frequency includes dissipative effects and is expressed as $\omega_r =$

$\omega_0\sqrt{1-\left(\frac{\gamma}{2m\omega_0}\right)^2} = \frac{2\pi}{T_r}$, and T_r is the period of the resonance. Such a system is characterized by the following second order differential equation:

$$m\ddot{x} + \gamma\dot{x} + kx = F_1 + F_{dr}(t), \qquad (1)$$

where $F_{dr}(t)$, represents harmonic forcing. The response takes the general form

$$x(t) = \frac{F_1}{k} + e^{-\frac{\gamma}{2m}t}e^{-it\omega_0\sqrt{1-\left(\frac{\gamma}{2m\omega_0}\right)^2}}\left(a + e^{-2it\omega_0\sqrt{1-\left(\frac{\gamma}{2m\omega_0}\right)^2}}b\right)$$
$$+ F_{dr}\frac{m(\omega_0^2-\omega_{dr}^2)\sin(\omega_{dr}t)-\gamma\omega_{dr}\cos(\omega_{dr}t)}{(\gamma\omega_{dr})^2+m^2(\omega_0^2-\omega_{dr}^2)^2}, \qquad (2)$$

All the simulations outlined above can be expressed by applying the driving conditions and the boundary conditions and solving for the integration constants a and b. Without loss of generality we define the target amplitude to be x_0, which is reached by the steady state force $F_0 = kx_0$.

For example, the ring free set-up depicted in Figure is obtained by setting $F_{dr} = 0$, $x(0) = 0$ and $x'(0) = 0$. The last free parameter is F_1, which is determined by requiring that the apex is reached after the first half period, or $x(t_1) = x_0$, note that $t_1 = \frac{1}{2}T_r$. The solution is the well-known expression for the response of a harmonic oscillator to the step drive:

$$x(t) = \frac{F_1}{k}\left(1 - e^{-\frac{\gamma t}{2m}}\left(\cos(\omega_r t) + \frac{\gamma}{2m}\sin(\omega_r t)\right)\right), \qquad (3)$$

and the force taking the form

$$F_1 = F_{st-up} = F_0\left(1 - \frac{1}{1+e^{\frac{\gamma}{2m}t_1}}\right)$$
$$\approx \frac{F_0}{2}\left(1 + \frac{\pi}{4Q}\right) + O[Q^{-2}], \qquad (4)$$

where the latter expression is valid in the high Q limit.

Once the apex is reached the forcing can be turned to F_0 to hold the position x_0 at rest, as is illustrated in Figure . Alternatively, in scanning mode, a unipolar square wave can be applied to maintain the amplitude of the oscillating response. A plot of the drive force and response are illustrated in Figure 9 for a $Q = 10$ system and is constructed in the following way:

I)   The step-up is expressed by equation 3 displaced by time t_0 so that $t \to (t - t_0)$ and the drive force is F_{st-up} given by equation 4. The step-up duration lasts= t_1. or half a period of the damped system. In the high Q limit (introducing an error on the order of 0.2% for $Q=10$) equation 3 becomes

$$x(t) = \frac{F_1}{k}\left(1 - e^{-\frac{\gamma(t-t_0)}{2m}}\cos(\omega_r(t - t_0))\right), \qquad (5)$$

II)   The response is set to ring for $N=6$ full periods or $T_N = 6T_r = \frac{6}{f_r}$, after which a final pulse pulls all the energy out of the mode so that the resonator comes to rest at the origin. In a dissipationless system the forcing and response is symmetric. Including dissipation results in a second pulse which is smaller than the first as some of the energy is dissipated and does not need to be actively pulled out of the mode. One finds that the step-down force is

$$F_1 = F_{st-dn} = F_0 - F_{st-up} = \left(\frac{F_0}{1+e^{\frac{\gamma}{2m}t_1}}\right)$$
$$\approx \frac{F_0}{2}\left(1 - \frac{\pi}{4Q}\right) + O[Q^{-2}], \qquad (6)$$

and the amplitude response takes the form

$$x(t) = \frac{F_0}{k} - \frac{F_1}{k}\left(1 - e^{-\frac{\gamma t}{2m}}\left(\cos(\omega_r t) + \frac{\gamma}{2m}\sin(\omega_r t)\right)\right), \qquad (7)$$

$$x(t) = \frac{F_{st-dn}}{k} + \frac{F_{st-up}}{k}e^{-\frac{\gamma t}{2m}}\cos(\omega_r t),$$

with the time shifted to $t_{dn} = t - t_0 - t_1 - t_N$ and the second expression holds for large Q.

III)   The cyclic period, in the example given here lasting 6 periods, is determined by solving equation 1 with $F_{dr}=0$ and F_1 switching on and off to form a uni-polar square wave with frequency $f_r = \frac{1}{T_r}$ and amplitude F_{SqW}. As two time-sections are implemented two sets of boundary conditions are needed: Initially, $F_1 =0$ $x_a(t_1) = x_0$, and $x_a'(t_1) = 0$, corresponding to
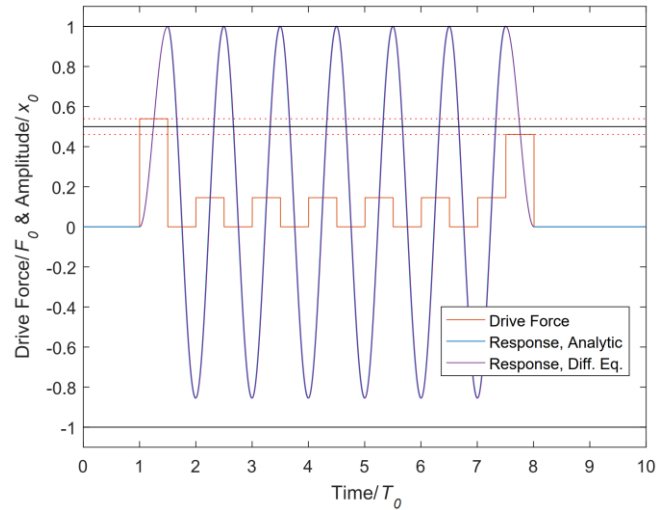

Figure 9 *Shown is the response for a system with a Q of 10 with the applied pulse train in red (square wave unipolar drive). The analytic solution reproduces perfectly the numeric solution to the differential equation. The black line illustrates the amplitude of the first and last pulse for a dissipation free system, the dashed lines illustrate the drive forces needed to add and remove the energy from the mode.*

a release from rest at position x_0. A half-period later, $\frac{1}{2f_r}$, the force is switched to F_{SqW}.

The boundary conditions ensure a smooth continuity: $x_b\left(t_1 + \frac{T_r}{2}\right) = x_a\left(t_1 + \frac{T_r}{2}\right) = -x_0 e^{-\frac{\gamma\pi}{2m\,\omega_r}}$. and $x_b'\left(t_1 + \frac{T_r}{2}\right) = 0$. Finally, the force, F_{SqW}, needed to reach the target amplitude x_0 is determined by the condition that the apex is reached after a further half period, such that $x_b(t_1 + T_r) = x_0$. The sequence repeats N times until the energy is pulled from the mode as described previously. A closed form is given as:

$$x_a(t_a) = e^{-\frac{\gamma t_a}{2m}}\cos(\omega_r t_a) \qquad \left[0 < t_a < \frac{T_r}{2}\right]$$

(8)

$$x_b(t_b) = -e^{-\frac{\gamma t_b}{2m}}\cos(\omega_r t_b) + x_0 \qquad \left[0 < t_b < \frac{T_r}{2}\right]$$

With $t_a = \mathrm{mod}(t - t_0 - t_1, T_r)$ and $t_b = \mathrm{mod}\left(t - t_0 - t_1 - \frac{T_r}{2}, T_r\right)$, and $t \in \left[t_0 + \frac{1}{2}T_r, t_0 + \left(N + \frac{1}{2}\right)T_r\right]$. Finally, the force required to remain "topped off" with a square wave drive is

$$F_{SqW} = F_0\left(1 - \frac{1 + e^{-\frac{\gamma\pi}{2m\,\omega_r}}}{1 + e^{\frac{\gamma\pi}{2m\,\omega_r}}}\right)$$

(9)

$$\approx F_0\frac{\pi}{2\,Q}\left(1 - \frac{\pi}{4\,Q}\right) + \mathrm{O}[Q^{-3}].$$

Figure 9 is generated by combining the results for the drive from equations 4 and 6 to generate the forcing for the step-up and down respectively, and equation 9 to maintain the resonant response. The amplitude response of the drive is plotted using equations 5, 7, and 8. The forcing starts at $t_0=1$ and the time is normalized to the period of the resonator. The solid black trace indicates the level of the step up and step-down forces for a dissipation free system, where for such a case no square-wave drive would be needed. As the forcing is only in one direction the response is no longer symmetric in amplitude with the negative deflection only reaching an amplitude of $-x_0 e^{-\frac{\gamma\pi}{2m\,\omega_r}}$. A numeric solution of the differential equation 1 is indistinguishable from the analytical solution.

The same exercise can be repeated for a harmonic drive, where now $F_l=0$ and F_r is determined by applying the boundary conditions. The response due to the harmonic drive force, $F_{r-up}\sin(\omega_r t)$, is given by the ring up expression

$$x(t \to t - t_0) = A_t e^{-\frac{\gamma t}{2m}}\sin(\omega_r t + \varphi_t)$$

$$+A\cos(\omega_r t + \varphi),$$

(10)

with the steady state terms $\varphi = \tan^{-1}\left(\frac{m\omega_r}{\gamma}\right) + \frac{\pi}{2}$ and $A = \frac{F_0}{m}\frac{1}{\sqrt{(\omega_0{}^2 - \omega_r{}^2)^2 + \left(\frac{\gamma\omega_r}{m}\right)^2}}$, and the transient terms $\varphi_t = \tan^{-1}\left(\frac{\omega_r}{\frac{\gamma}{2m} + \omega_r\tan\varphi}\right)$ and $A_t = -A\frac{\cos\varphi}{\sin\varphi_t}$. When removing energy after the steady state oscillations the amplitude response becomes

$$x(t \to t - t_0 - (N+1)T_t) = -A_t e^{\frac{\gamma t}{2m}}\sin(\omega_r t - \varphi_t)$$

$$+ A\cos(\omega_r t - \varphi),$$

(11)

applicable for $t \in \left[t_0 + \left(N + \frac{1}{2}\right)T_r, t_0 + (N + 1)T_r\right]$. The expressions for the ring up and ring down forcing amplitudes are

$$F_{r-up} = F_0\frac{x_0}{A_t e^{-\frac{\gamma}{2m\omega_r}\pi}\sin(\pi + \varphi_t) + A\cos(\pi + \varphi)}$$

$$\approx F_0\left(\frac{2}{\pi} + \frac{1}{2Q}\right) + \mathrm{O}[Q^{-2}],$$

(12)

and

$$F_{r-dn} = \frac{F_0 m}{\gamma\,\omega_r\,\omega_0{}^2}\frac{\left(\left(\frac{\gamma\omega_r}{m}\right)^2 + \left(\frac{\gamma}{2m}\right)^4\right)}{\left(e^{\frac{\pi\gamma}{2m\omega_r}} - 1\right)}$$

$$\approx F_0\left(\frac{2}{\pi} - \frac{1}{2Q}\right) + \mathrm{O}[Q^{-2}].$$

(13)
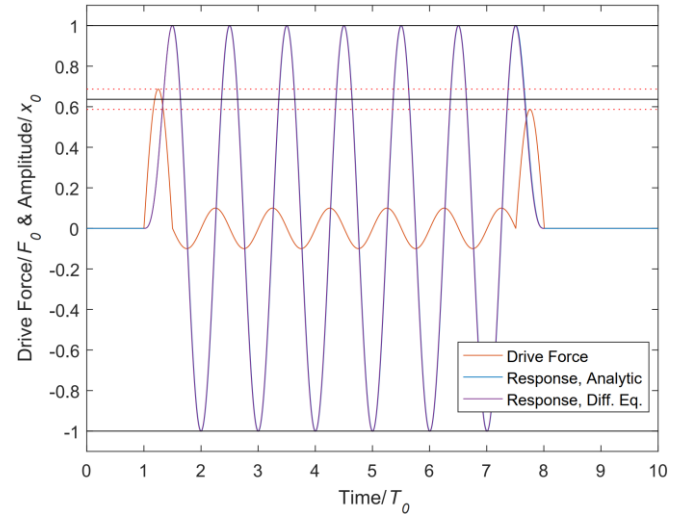
During the steady state the amplitude is

Figure 10 Sine wave drive. A first and last half period sine drive rapidly dumps and extracts energy from the mode. To maintain the mode amplitude a resonant drive is applied. The plot describes a Q=10 system, the analytic result perfectly matches the numeric solution for the differential equation. The black line illustrates the amplitude of the first and last pulse for a dissipation free system, the dashed lines illustrate the drive forces needed to add and remove the energy from the mode.

$$x\left(t \to t - t_0 - \frac{1}{2}T_t\right) = Q\frac{F_0}{k}\cos(\omega_r t), \qquad (14)$$

with $t \in \left[t_0 + \frac{1}{2}T_r, t_0 + \left(N + \frac{1}{2}\right)T_r\right]$ and the harmonic forcing is simply
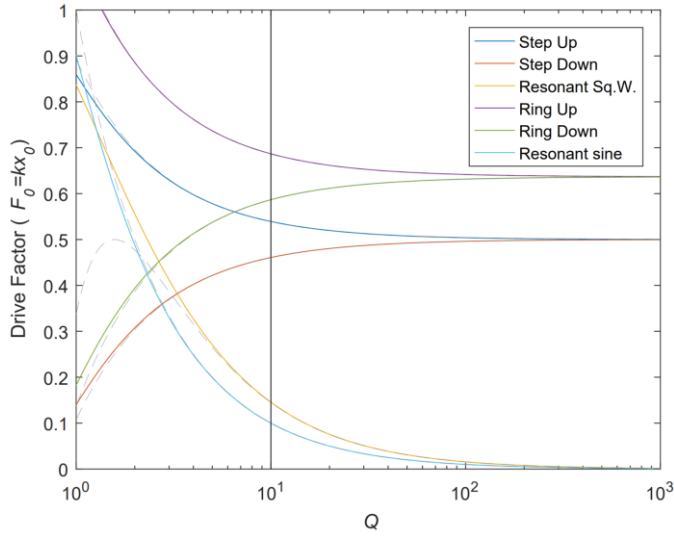

Figure 11 *Normalized drive forces depending on drive method as a function of the Quality factor. In each case the response amplitude is normalized to $x_0 = \frac{F_0}{k}$. The yellow and light blue trace illustrate the drive force needed to maintain the amplitude of the resonant system for a unipolar square wave and resonant sine wave drive respectively. As would be expected these fall off with increasing Q as the need to "top off" vanishes. The step up and step-down amplitude converge at 0.5 for the step drive and at $\frac{2}{\pi}$ for the sine drive. In both cases the step-down force vanishes for low Q as all the energy in the mode is removed by dissipation and no breaking force is needed. The solid vertical black line corresponds to Q = 10, for which system the full responses are illustrated in figures 9 and 10.*

$$F_{dr}(t) = \frac{F_0}{m} \frac{1}{\sqrt{(\omega_0^2 - \omega_r^2)^2 + \left(\frac{\gamma\omega_r}{m}\right)^2}} \sin(\omega_r t + \pi)$$

$$\tag{15}$$

$$\approx \frac{F_0}{Q} \sin(\omega_r t + \pi).$$

The drive force and the response of the bi-polar harmonic drive is illustrated in Figure 10 for a Q=10 system. Again, the analytic solution presented here is indistinguishable from the numeric solution of the differential equation. An advantage of this drive modality is the symmetric bi-polar response. It should be noted that a harmonic oscillation which is only in the positive regions can easily be generated by replacing the steady state drive with a dc offset and half the resonant force. Such that

$$F_{dr}(t) = \frac{F_0}{2}\left(1 + \frac{1}{Q}\sin(\omega_r t + \pi)\right). \tag{16}$$

Figure 11 illustrates how the different forcing amplitudes, scaled to the static force F_0, are affected by the quality factor. As would be expected the steady state forces, for both the harmonic and square wave drive fall off for high Q. For high Q the step-up/ring-up forces and step-down/ring-down forces respectively also converge as would be expected for a reversible dissipation free system. The step-down/ring-down force amplitudes vanish for low Q, as for such systems all energy is

dissipated passively and there is no longer the need to actively apply a breaking force.

IV. EXPERIMENTAL RESULTS

To demonstrate these effects on a MEMS device, we have used a commercial micro-mirror system, the Mirrorcle Technologies product [20]. The device and system are shown in Figure . The device we used has a 5mm diameter mirror, a resonant frequency of 325 Hz and a packaged Q of 25. It is a Mirrorcle model A8L2.2 mirror, gimbal-less two axis bonded design with a gold-coated mirror and a tip/tilt range of +/- 5 degrees about two axes.

Figure 12 also shows our experimental setup. The mirror is solidly mounted in the center of the system and a laser and position sensitive detector are used to measure the mirror angles of rotation. For these experiments, we only use one axis of rotation. The mirror is controlled by an electronic drive circuit that determines the mirror angle. A +/- 10 V input creates a +/- 5 degree rotation. The actual MEMS device itself is operated with ~180 volts of drive. The electronic circuit has a look-up table with the device calibration stored on it and this system both creates the high voltage needed and corrects for the quadratic voltage dependence normally seen for a MEMS device. The input voltage to the system (+/- 10 V) produces a linear angular response (+/- 5 degrees) and so the input can be thought of as a force directly applied to the mirror. The electronic circuit is thus designed and calibrated to act like a fixed angular spring constant. The circuit is well fast enough to respond to the dynamics being studied here. An analog multiplier circuit (AD633) was used to modulate the input signal along with an SRS summing circuit to add the various pulses together, created by an SRS DG645 pulse generator.
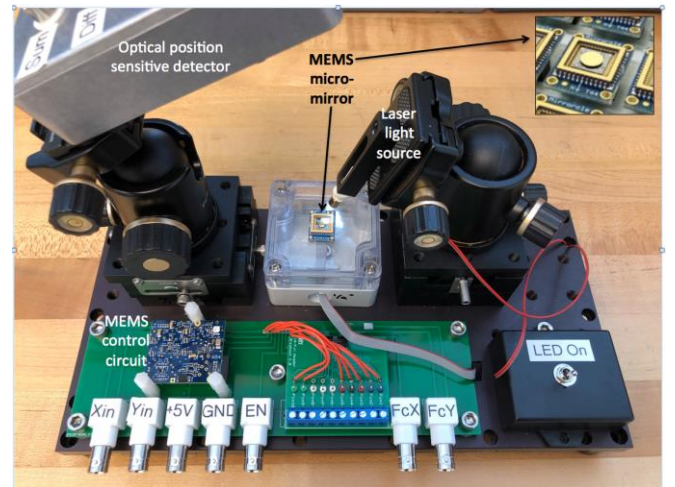

Figure 12 *Shown is our experimental apparatus. The Mirrorcle MEMS micro-mirror is mounted on the central section, illuminated with a laser and the position sensitive detector is used to detect the mirror's angular position. The mirror is controlled by an electronic circuit shown in the lower left of the photo.*
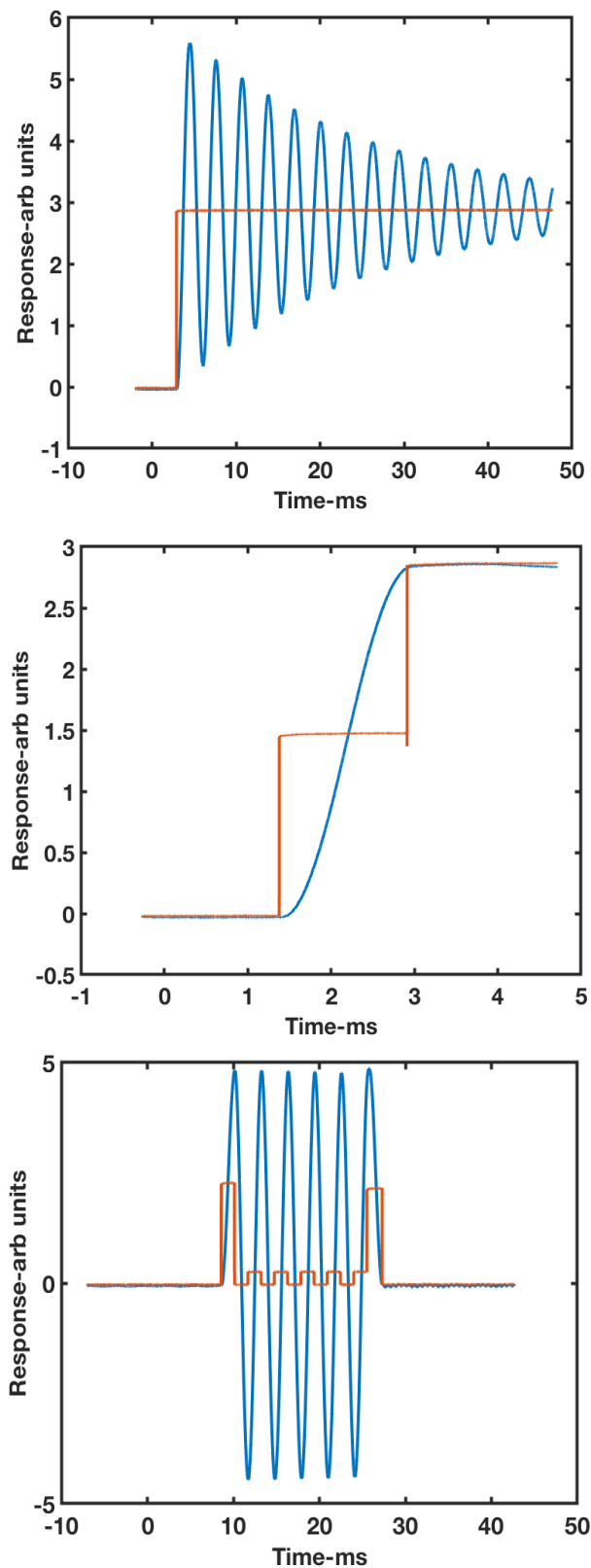
Figure 13 shows our experimental results. In the top panel, we show the native response of the system to a single step input. The $Q\sim25$ and the system rings for many tens of milliseconds. The middle panel shows the response to a two-step input, similar to the simulations shown in Figure 1 and the analytical solutions shown in Figure 8. In the two-step input the settling time has been reduced to ~1/2 a period or ~1.5 ms. The lower panel shows the response to a more complicated drive, similar to that drive algorithms can make this device function as an essentially perfect galvo and a perfect scanner. **Error! Reference source not found.**14 shows how, by bringing all the algorithms together on a real MEMS device, one can modal engineer the output to create complex patterns. The experimental results in **Error! Reference source not found.**14 can be compared with the simulation results in Figure 4. They agree, demonstrating the effectiveness of the algorithms discussed   here.
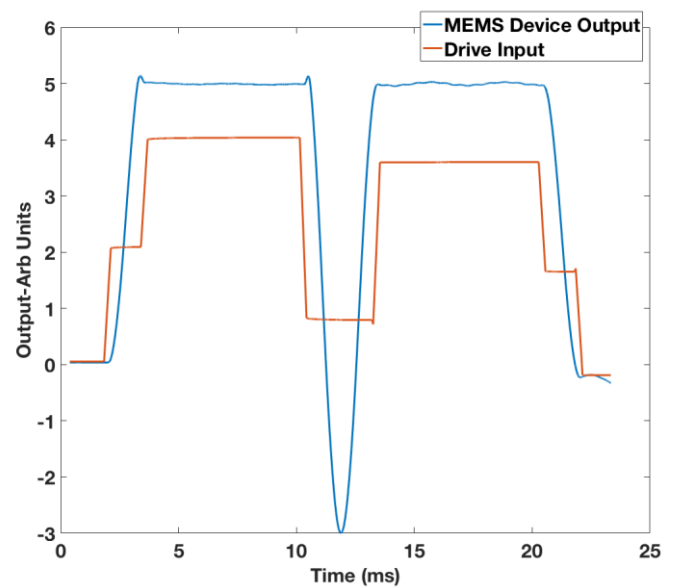

Figure 14 Shown is a complex pattern of response of the MEMS device shown in Figure 12. This is a similar pattern to that shown in Figure 4.

V. CONCLUSIONS

In this paper we have shown how novel open loop control algorithms can make MEMS devices perform as essentially ideal galvos and scanners. In a real device, with a finite Q, changes to the input cause the system to ring and the response time is not ideal. For an optical system, this is wasted time because the device is not in a well-defined state. Using the algorithms shown here, one can make an imperfect device perform in an essentially ideal manner.

We believe that the algorithms we have presented here will allow for the optical system designer to make a better use of the imaging time with minimal overhead due to MEMS device ringing and settling.

ACKNOWLEDGMENT

Figure 13 Shown are results on the Mirrorcle MEMS micromirror using the algorithms described in the text. The red curve is the drive and the blue curve the device response. The upper panel shows the native response of the device. In response to a step input, it rings for ~100ms. The middle panel shows the step response reduced to ~1ms and the lower panel shows how one can use an advanced drive method to produce ideal scanner behavior. Note the differing time scales in all three plots.

REFERENCES

[1] D. J. Bell, T. J. Lu, N. A. Fleck, and S. M. Spearing, "MEMS actuators and sensors: observations on their performance and selection for purpose," *J. Micromechanics Microengineering*, vol. 15, no. 7, pp. S153–S164, Jul. 2005.

[2] C. Liu, *Foundations of MEMS*, 2nd ed. Prentice Hall, 2012.

[3] M. K. Mishra, V. Dubey, P. M. Mishra, and I. Khan, "MEMS Technology: A Review," *J. Eng. Res. Reports*, pp. 1–24, Feb. 2019.

[4] S.-C. Chen and M. L. Culpepper, "Design of a six-axis micro-scale nanopositioner μHexFlex," *Precis. Eng.*, vol. 30, no. 3, pp. 314–324, Jul. 2006.

[5] M. Imboden *et al.*, "Atomic Calligraphy: The Direct Writing of Nanoscale Structures Using a Microelectromechanical System," *Nano Lett.*, vol. 13, no. 7, pp. 3379–3384, Jul. 2013.

[6] L. K. Barrett *et al.*, "A Large Range of Motion 3D MEMS Scanner With Five Degrees of Freedom," *J. Microelectromechanical Syst.*, pp. 1–10, 2019.

[7] C. Pollock, J. Javor, A. Stange, L. K. Barrett, and D. J. Bishop, "Extreme angle, tip-tilt MEMS micromirror enabling full hemispheric, quasi-static optical coverage," *Opt. Express*, vol. 27, no. 11, p. 15318, May 2019.

[8] S.-C. Chen, M. L. Culpepper, and S. C. Jordan, "Application of Input Shaping and HyperBit Control to Improve the Dynamic Performance of a Six-axis MEMS Nano-positioner," in *ASPE 2006*, 2006.

[9] V. Milanović and K. Castelino, "Sub-100 μs Settling Time and Low Voltage Operation for Gimbal-less Two-Axis Scanners," in *IEEE/LEOS Optical MEMS 2004*, 2004.

[10] S. T. S. Holmström, U. Baran, and H. Urey, "MEMS laser scanners: A review," *Journal of Microelectromechanical Systems*, vol. 23, no. 2. Institute of Electrical and Electronics Engineers Inc., pp. 259–275, 2014.

[11] J. B. Hopkins, R. M. Panas, Y. Song, and C. D. White, "A High-Speed Large-Range Tip-Tilt-Piston Micromirror Array," *J. Microelectromechanical Syst.*, vol. 26, no. 1, pp. 196–205, Feb. 2017.

[12] D. N. Burghes and A. Graham, "Introduction to control theory, including optimal control." Horwood, 1980.

[13] F. L. Lewis, *Optimal Control*, 1st ed. Wiley, 1986.

[14] H. W. Yoo *et al.*, "MEMS-based lidar for autonomous driving," *Elektrotechnik und Informationstechnik*, vol. 135, no. 6, pp. 408–415, Oct. 2018.

[15] D. Wang, C. Watkins, and H. Xie, "MEMS Mirrors for LiDAR: A Review," *Micromachines*, vol. 11, no. 5, p. 456, Apr. 2020.

[16] M. Imboden *et al.*, "High-Speed Control of Electromechanical Transduction: Advanced Drive Techniques for Optimized Step-and-Settle Response of MEMS Micromirrors," *IEEE Control Syst.*, vol. 36, no. 5, pp. 48–76, Oct. 2016.

[17] C. Pollock *et al.*, "Engineered PWM Drives for Achieving Rapid Step and Settle Times for MEMS Actuation," *J. Microelectromechanical Syst.*, vol. 27, no. 3, pp. 513–520, Jun. 2018.

[18] C. Pollock, L. K. Barrett, P. G. del Corro, A. Stange, T. G. Bifano, and D. J. Bishop, "PWM as a Low Cost Method for the Analog Control of MEMS Devices," *J. Microelectromechanical Syst.*, pp. 1–9, 2019.

[19] A.-Q. Liu *et al.*, "Open-loop versus closed-loop control of MEMS devices: choices and issues," *J. Micromech. Microeng*, vol. 15, pp. 1917–1924, 2005.

[20] "Mirrorcle Technologies MEMS Mirrors – Technical Overview," 2013. Also https://www.mirrorcletech.com/wp/